Science Translational Medicine
AAAS

www.sciencetranslationalmedicine.org/cgi/content/full/9/394/eaah6144/DC1

Supplementary Materials for

Drugging the catalytically inactive state of RET kinase in RET-rearranged tumors

Dennis Plenker, Maximilian Riedel, Johannes Brägelmann, Marcel A. Dammert, Rakhee Chauhan, Phillip P. Knowles, Carina Lorenz, Marina Keul, Mike Bührmann, Oliver Pagel, Verena Tischler, Andreas H. Scheel, Daniel Schütte, Yanrui Song, Justina Stark, Florian Mrugalla, Yannic Alber, André Richters, Julian Engel, Frauke Leenders, Johannes M. Heuckmann, Jürgen Wolf, Joachim Diebold, Georg Pall, Martin Peifer, Maarten Aerts, Kris Gevaert, René P. Zahedi, Reinhard Buettner, Kevan M. Shokat, Neil Q. McDonald, Stefan M. Kast, Oliver Gautschi, Roman K. Thomas, Martin L. Sos*

*Corresponding author. Email: martin.sos@uni-koeln.de

Published 14 June 2017, *Sci. Transl. Med.* **9**, eaah6144 (2017)
DOI: 10.1126/scitranslmed.aah6144

This PDF file includes:

Materials and Methods

Study population

Informed consent was obtained from all patients, and IRB approval was available for genetic studies. *RET* FISH testing was performed by experienced pathologists (RB, JD) as described before *(35)*. All tumors were negative for coexisting mutations of *EGFR*, *ALK*, *ROS1*, *HER2*, or *BRAF*. Rebiopsies of P1 and P2 were sequenced using hybrid capture-based next-generation sequencing (NEO, New Oncology AG). Available RET inhibitors were given off-label (sunitinib, vandetanib) or compassionate use (cabozantinib) in accordance with local regulations. Follow up was performed by PET or CT scans in intervals of 2-4 weeks, and interpreted by radiologists. Response rates were measured according to RECIST 1.1 criteria.

Antibodies used for immunoblot

The following antibodies were obtained from Cell Signaling: p-AKT Ser473 (Catalog No. #9271), p-ERK1/2 Thr202/Tyr204 (Catalog No. #4370), p-S6 Ser235/236 (Catalog No. #4858), p-RET Tyr905 (Catalog No. #3221), AKT (Catalog No. #9272), ERK 1/2 (Catalog No. #9102), S6 (Catalog No. #2217), RET (Catalog No. #3220). HSP90 (#SPA-835) was purchased from Enzo.

Antibodies were diluted in TBST containing 5% milk (Carl Roth) and incubated at 4°C overnight on a shaker. Actin as a loading control was detected via an actin-horseradish peroxidase (HRP) antibody (Santa Cruz Biotechnology, Catalog No. #sc47778). Detection of proteins was performed via HRP-conjugated anti-mouse anti-rabbit antibodies (Millipore) via enhanced chemiluminescence (ECL) reagent (GE Healthcare) or via near infrared fluorescent dye coupled antibodies (LI-COR

Biosciences). Due to overlapping molecular weights, not all proteins were detected at the same membrane per displayed figure panel.

Cell culture

LC-2/AD [RPMI:HAMS F12 (1:1), 2 mM glutamine (LifeTechnologies)] cells were obtained from Sigma Aldrich. TPC-1 (cultured in RPMI) cell line and Ba/F3 (cultured in RPMI) murine pro-B cell line were gifts (see acknowledgements). NIH-3T3 (cultured in DMEM) murine fibroblast cell line was purchased from DSMZ. All cell lines were grown in a humidified incubator in medium supplemented with 10% fetal bovine serum and 1% penicillin-streptomycin (LifeTechnologies) at 37 °C and 5% CO_2.

Viability and colony formation assays

3,000 (adherent) or 10,000 cells (suspension) for viability assays in 96-well plates and 10,000 cells for colony formation assays in 12-well plates were used and analyzed as previously described *(40)*. GI_{50}-values were determined with GraphPad Prism 6.0h.

Molecular cloning and viral transduction

Full length *KIF5B-RET* and *CCDC6-RET* were cloned in the retroviral vector pBabe-puro (Addgene #1764) via Gibson assembly (NEB). KRAS-G12V was cloned via Gibson Assembly into the pLenti6 backbone (Thermo Scientific). Site-directed mutagenesis was performed using Q5 polymerase (NEB). Mutations and analysis of complete inserts were confirmed via Sanger sequencing at the Cologne Center for Genomics. pBabe and pLenti vectors were co-transfected with corresponding helper plasmids with TransIT-LT1 (Mirus) using standard procedures in HEK293T cells.

After several passages, we observed a decrease in fitness of *KRAS*^{G12V} transduced LC-2/AD cells.

Undirected mutagenesis

The cDNAs of *CCDC6-RET* and *KIF5B-RET* were cloned into the pBabe puro backbone. Undirected mutagenesis was performed via *E. coli* XL1-Red (Stratagene) bacteria cells for 24/48/72 h as previously described *(24, 25)*. After viral transductions in Ba/F3 cells, cells were challenged with 200 nM AD80. After outgrowth, genomic DNA was isolated and sequenced using capture-based sequencing (CAGE) at NEO oncology.

FISH

Tumor specimens were stained with KIF5B, and RET break-apart FISH probes were purchased from Zytovision. For each case, 100 carcinoma cells were analyzed for rearrangements. Positivity was defined as ≥ 20% of cells showing aberrant patterns indicative of KIF5B / RET rearrangements: i) one break-apart (isolated red and isolated green signal) and one or more fusion signals, or ii) one or more isolated green signals and one or more fusion signals.

Phosphoproteomal analysis

Materials

If not mentioned otherwise, chemicals were purchased from Sigma Aldrich in the highest purity available. ULC-MS acetonitrile (ACN), formic acid (FA), and trifluoroacetic acid (TFA) were from Biosolve BV. Ultra-pure water was obtained from an ELGA Purelab flex water purification system (ELGA Labwater). C18 solid

phase extraction was conducted using SPEC C18-AR cartridges (Agilent Technologies).

Proteomics sample preparation

Protein concentrations of cell lysates were determined by a Pierce bicinchoninic-acid assay kit (Thermo Fisher Scientific) according to the manufacturer's instructions. To degrade DNA, samples were treated with 25 U Benzonase (Merck) in the presence of 2 mM $MgCl_2$ and incubated at 37 °C for 30 min. Cysteines were reduced with 10 mM dithiothreitol (DTT) for 30 min at 56 °C. Afterwards, free cysteines were alkylated with 30 mM iodoacetamide (IAA) for 30 min at RT in the dark. Excess IAA was quenched by addition of 10 mM DTT for 15 min. Proteolytic digestion was conducted using a modified filter aided sample preparation procedure*(43)*: for each sample, 150 µg of protein was diluted with freshly prepared 8 M urea, 100 mM TRIS buffer (pH 8.5) to a final concentration of 7 mM SDS and 6.4 M urea *(44)*. Samples were passed over 30 kDa Pall Nanosep Omega molecular weight cut off centrifuge filters (VWR International) by centrifugation for 25 min at 13,500 g, followed by three washing steps with 8 M urea, 100 mM TRIS, pH 8.5, and another three steps with 50 mM triethylammonium bicarbonate buffer (TEAB, pH 8.5). Trypsin (sequencing grade modified, Promega) was added in a 1:25 ratio in 150 µL of 50 mM TEAB, 0.2 M guanidine hydrochloride, and 2 mM $CaCl_2$, and samples were incubated at 37°C for 14 h. Generated peptide mixtures were collected from the filters by centrifugation, followed by two washing steps with 50 µL of 50 mM TEAB and H_2O, respectively. Samples were acidified to pH ~2.0 with TFA, and 1 µg per sample was used to control digest efficiency and reproducibility as described elsewhere *(45)*.

TMT labeling, multiplexing, and sample cleanup:

A mixed sample containing 150 µg of peptide was generated using equal amounts of the 9 different conditions. Afterwards, 150 µg per sample were labeled with TMT 10-plex reagents (Thermo Fischer GmbH) according to the manufacturer's protocol (controls: 126, 127N, 127C; 10 nM AD80: 128N, 128C, 129N; 100 nM AD80: 129C, 130N, 130C; mixed sample: 131). After labeling and quenching with 5% hydroxylamine, samples were multiplexed, dried under vacuum, and reconstituted in 300 µL of 0.1% TFA. Next, samples were desalted on a 50 mg SPE cartridge, and an aliquot corresponding to 40 µg of peptides was taken for global proteome analysis (see below).

Phosphopeptide enrichment and fractionation

Phosphopeptides were enriched by TiO_2 with slight modifications *(46)*. Briefly, the multiplexed sample was incubated in 5% TFA, 80% ACN, 1 M glycolic acid together with an excess of TiO_2 beads 3 times (beads to peptide ratios were 1:6, 1:3 and 1:1.5), and peptides were eluted from the beads with 1.12% NH_4OH. A second sequence of incubations with the same amounts of fresh TiO_2 beads in 70% ACN, 2% TFA was performed to achieve maximum enrichment specificity. The phosphopeptide-enriched sample was desalted using Oligo R3 (Applied Biosystems) *(41)*. Phosphopeptides were reconstituted in HILIC loading buffer (98% ACN, 0.1% TFA) and directly fractionated by hydrophilic interaction liquid chromatography (HILIC) on an Ultimate 3000 RSLCnano system (Thermo Fisher Scientific) equipped with a self-packed 250 µM x 15 cm column filled with TSK GelAmide 80 material (3 µM, 100 Å, Tosoh Bioscience GmbH). A 37 min gradient from 10-35% of 0.1% TFA was used to obtain a total of 16 fractions for LC-MS/MS analysis.

High-pH reversed phase fractionation:

For the global proteome analysis, 40 µg of labeled peptides were fractionated by high pH RP chromatography using an UltiMate 3000 HPLC (Thermo Fisher Scientific). The peptide sample was redissolved in 10 mM ammonium formate (pH 8.0, adjusted with FA) and separated on a BioBasic C18 column (500 µM x 15 cm, 5 µM, 300 Å, Thermo Fisher Scientific) with a flow rate of 12.5 µL/min at 30 °C using a gradient from 3-50% of 10 mM ammonium formate, 84% ACN, pH 8.0 in 70 min. Fractions were collected between 10 and 80 min in concatenation mode (1 min intervals) to yield a total of 20 fractions. Fractions were dried under vacuum and reconstituted in 32 µl of 0.1% TFA. 50% per fraction were subjected to LC-MS/MS analysis.

Nano LC-MS/MS analysis

Nano LC-MS/MS was conducted on an Ultimate 3000 RSLCnano system equipped with Acclaim PepMap C18 columns (precolumn: 100 µM x 2 cm, 5 µM, 100 Å; main column: 75 µm x 50 cm, 3 µM, 100 Å; both Thermo Scientific). Samples were reconstituted in 0.1% TFA and trapped on the precolumn for 10 min at a flow rate of 20 µl/min 0.1% TFA. Peptides were separated using a binary gradient and solvents A (0.1% FA) and B (84% ACN, 0.1% FA) ranging from 3-35% B for either 60 min (phospho) or 90 min (global and phospho). The HPLC was connected online to a Q-Exactive HF mass spectrometer (Thermo Fisher Scientific) via a nano-ESI interface in positive ion mode, and samples were analyzed in data-dependent acquisition mode (DDA). Survey scans were acquired with a resolution of 60,000, an AGC target value of 1×10^6, and a maximum injection time of 120 ms. The top 15 most intense signals with charge states 2-5 were subjected to MS/MS using dynamic exclusion of 30 s, an isolation width of 0.8 *m/z*, a normalized collision energy of 33%, a resolution of 60,000, an automatic gain control target value of 2×10^5, and a maximum injection time of 200 ms, with the first mass set to 100 *m/z*. To compensate for a higher

complexity of the global proteome fractions, the isolation width was reduced to 0.4 *m/z* to reduce the potential precursor co-isolation.

Data analysis:

All raw files were searched against the human Swiss-Prot database (www.Uniprot.org; April 2016, 20,207 target sequences) using Mascot v 2.4.1 (Matrix Science) and the Proteome Discoverer 1.4 software package (Thermo Fisher Scientific). Search settings were as follows. (i) Trypsin was used as enzyme with (ii) with a maximum of 2 missed cleavage sites. Mass tolerances were (iii) 10 ppm for precursors and (iv) 0.02 Da for fragment ions. (v) TMT 10-plex (+229.163 Da on Lys and N-termini) and carbamidomethylation of Cys (+ 57.021 Da) were set as static modifications. (vi) Phosphorylation of Ser/Thr/Tyr (+ 79.966 Da) and oxidation of Met (+ 15.995 Da) were set as dynamic modifications. Phosphorylation site confidence was determined using phosphoRS 3.1, and false discovery rate assessment was performed using Percolator *(47, 48)*. For the phosphopeptide data analysis, only unique peptide-spectrum-matches (PSMs) with high confidence (< 1% FDR), a search engine rank of 1, and a minimum phosphoRS site localization probability of 0.9 for all sites were considered. For the global proteome, only proteins quantified with at least 2 unique high confidence peptides were considered. Sorting and evaluation of the exported data as well as calculations were done in Microsoft Excel 2013.

Global proteome: Because Proteome Discoverer only provided 9 ratios for the 10 samples, an artificial 126/126 ratio was created and set to 1.0 per protein. For each channel, a median overall protein log2-ratio was calculated ($MD1_{126\text{-}131}$). Next, the median over all ten MD1 values was determined (MD2) to define normalization values (NV) per channel, and these MD2 were subtracted from the individual MD1

values. This normalization was performed to compensate for individual systematic errors (unequal sample amounts derived from pipetting errors or inaccurate BCA results) and to obtain normalized log2-ratios (NR) per protein (126/126, 127/126, …, 131/126).

Next, for each protein, the median over all ten NRs was subtracted from the individual NRs to obtain scaled normalized abundance values (NAV) for all proteins and channels after retransformation to decadic values.

Per protein NAVs of the three biological replicates were summed and used to obtain protein ratios between different conditions (for example, for 10 nM AD80 vs. control: sum (128N,128C,129N)/sum(126,127N,127C)). Additionally, a Student's t-test (two sided, homoscedastic) was applied between the respective triplicate groups of NAVs for each comparison.

The global median (GM) and the global standard deviation (GSD) over all log-2 protein ratios were then calculated for each comparison, and values greater than GM + 3*GSD or smaller than GM - 3*GSD were considered as potentially regulated, if the corresponding p-value was ≤ 0.05.

Phosphoproteome: The NVs, GMs, and GSDs from the global proteome were used to process the phosphoproteomics data. First, for each TMT channel, the areas of all PSMs were divided by their respective NVs to yield normalized areas (NAs). The NAs for each PSM were then scaled by dividing them by the median over all ten NAs to yield the normalized abundance values of phosphopeptide-PSMs (p-NAVs). The p-NAVs of multiple PSMs corresponding to a specific phosphopeptide (same sequence, same phosphorylation site(s)) were averaged for each channel to obtain the averaged normalized abundance values of phosphopeptides ($p\text{-}NAV_{avr}$). The $p\text{-}NAV_{avr}$s were

used to obtain ratios between biological conditions, and corresponding p-values were determined as above. The ratios were subsequently log2-transformed. A phosphopeptide was considered as potentially regulated between conditions if (i) the log2 ratio was greater than GM + 3*GSD or smaller than GM - 3*GSD, (ii) the corresponding *p*-value was $\leq$0.05, and (iii) the corresponding protein was not regulated in the global proteome data to ensure that an apparent phosphorylation site regulation is not actually a change of expression during the 4 h stimulation experiment.

For computational prediction of kinases with altered activity from the differentially regulated phosphorylation sites observed in the phosphoproteome, we used the group based kinase prediction algorithm (GPS) version 2.1.2. *(49)*. The FASTA formatted sequences of proteins with regulated phosphorylation sites were provided to GPS (high confidence threshold) for kinase prediction. Per site, only the highest ranking high confidence kinase prediction was considered, and the altered phosphorylation sites per kinase were quantified.

Protein Thermal Shift assay (detailed description)

Constructs

Constructs were prepared as described previously *(17)*. In addition, ΔCCDC6-KD (residues 54 to 101 fused to RET 713 to 1012) and ΔKIF5B-KD (residues 544 to 757 fused to RET 713 to 1012) both including the D874N mutation to generate kinase dead constructs were ordered from Geneart (Life Technologies). Baculovirus production was carried out in the same manner as previously described *(17)*.

Protein production

SF21 cells were grown in SF-900 III SFX medium with 10 μg/ml gentamycin in shaker flasks at 27 °C for protein production. Viral infections were performed on high density cells (5 x 10^6 cells/ml) supplemented with 1% glucose (Sigma), 6.64 g/L yeastolate (Difco), and lactalbumin (Sigma). Cells were harvested 72 hours after infection, resuspended in lysis buffer (20 mM Tris pH 8.0, 150 mM NaCl, 1 mM DTT, 10 mM benzamidine, 0.2 mM AEBSF), lysed by sonication, and purified by incubation with glutathione-Sepharose 4B beads (Amersham Biosciences). Purified proteins were either dephosphorylated using 10 units of CIP (NEB) and 10 mM $MgCl_2$, or the core-KD and JM-KD were phosphorylated with 2.5 mM ATP and 10 mM $MgCl_2$. The immobilized ΔKIF5B-KD and ΔCCDC6-KD proteins were phosphorylated using purified solubilized JM-KD, 2.5 mM ATP, and 10 mM $MgCl_2$. Dephosphorylation and phosphorylation steps were all carried out for either 2 hours at RT or overnight at 4 °C. Proteins were subsequently washed and cleaved from resin using a GST-linked 3C protease. Purified ΔKIF5B-KD and ΔCCDC6-KD proteins were additionally purified by size exclusion chromatography on a Superdex 200 column, and all proteins were concentrated in HEPES buffer (20 mM HEPES pH 8.0, 150 mM NaCl, and 1 mM DTT) to 0.1 mg/ml.

Protein thermal shift

Control or drug-treated samples were incubated with DMSO or indicated drug at a final concentration of 1 μM, both to a final DMSO concentration of 1%, for up to 30 minutes on ice. Sypro-Orange dye (Life Technologies) was subsequently added and incubated for 5 min on ice before running the experiment. Quadruplicates of each sample per experiment were set up in MicroAmp Fast Optical 96-Well Reaction

Plates (Applied Biosystems), and plates were sealed and run in a 7500 Fast RT PCR machine (Applied Biosystems) with a temperature range of 25 – 90 °C. Data were analysed using the Protein Thermal Shift Software v1.2 (Applied Biosystems). Derivative melt curve plots were used for final data analysis to generate the proteins' melting point (Tm) and the difference in melting temperatures (ΔTm). Results were then averaged across experiments, and SEM values were calculated.

Computational binding mode modeling

Similar to the initial steps in *(20)*, we selected VEGFR (pdb code 2OH4 *(19)*) as template for modeling the relevant part of the wt RET protein due to the large sequence identity and availability of the DFG-*out* structure. Filling of sequence gaps and structure preparation was done using Modeller 9.14 *(50)*. An initial estimate of the wt binding mode for AD80 was created by superimposing the chemically equivalent part of AD80 with the so-called GIG ligand (pdb code 2OH4) as provided in the template structure file. Because to the best of our knowledge no cabozantinib structure bound to a kinase domain is deposited in the PDB, we generated an initial binding pose of cabozantinib to RET (wt) in a similar manner based on the final RET/AD80 model (see below). For that purpose, we took the chemically equivalent part of the XL880 ligand bound to the c-MET kinase (PDB code 3LQ8) and superimposed it onto the RET(wt)/AD80 complex followed by converting XL880 to cabozantinib. Two reasonable conformers of the quinoline ring system were initially created, and the energetically favorable geometry was selected after energy minimization in an implicit water model environment (ALPB) *(51)*. Amber ff99sb *(52)* was chosen as the protein force field, and we closely followed the preparation procedure outlined recently for the (assumed neutral) ligand models *(53)*.

All-atom molecular dynamics (MD) simulations for the RET complexes were performed by immersing them in 25428 (AD80) and 27987 (cabozantinib) TIP3P *(54)* water molecules after neutralizing with 8 chloride counterions using NAMD 2.10 *(55)* at a temperature of 298.15 K using a time step of 2 fs. MD runs were conducted in a sequence of steps to ensure stability. The simulation was initially performed for 4 ns in the canonical ensemble applying harmonic restraints on protein C^{α} atoms and the ligand, followed by 4 ns in the isothermal-isobaric ensemble (*NpT*) at 1 bar pressure to relax the volume. After lifting all restraints, we ran the simulation for an additional 92 ns in the isothermal-isobaric ensemble. We checked the stability of these completely free systems by monitoring root mean square deviations (RSMD, **fig. S5A**) from the initial structure, indicating sufficient stability. The resulting snapshot was optimized under ALPB conditions in Amber 12,*(52)* followed by point mutation by Modeller *(50)* to generate the V804M mutant. This structure was refined using a similar simulation protocol as for the wt, followed again by ALPB optimization. The initial structure for the RET(wt)/cabozantinib model was built based on the last frame of the RET(wt)/AD80 simulation, followed by further 112 ns in the *NpT* ensemble. The resulting snapshot was then treated in the same way as the RET/AD80 complexes.

The end point of the RET/AD80 simulation was used as the starting point for thermodynamic integration (TI) MD simulations, which were performed with pmemd in Amber 12 *(52)*. This was done in order to estimate the binding free energy difference between AD80 and AD57 in the presumed DFG-*out* bound protein conformation, which differ only by a single atom (F in AD80 is "alchemically," meaning by a continuous computational transformation, changed to H in AD57). Using MD settings as before, 11 consecutive coupling parameter (λ) windows ($\delta\lambda =$

0.1, 10 ns within each window) were simulated, dropping the initial 3 ns per window and using the remaining 7 ns for averaging in the isothermal-isobaric ensemble. To ensure correct physics, the transformed hydrogen atom of AD57 was excluded from the bond constraint algorithm.

In order to (roughly) estimate the binding free energy difference for AD80 bound to wt RET and to the V804M mutant, we performed single-state 3D RISM calculations on the final optimized structures, essentially following the methodology described in *(42, 56-58)*. Briefly, the optimized complex partners were separated, keeping their internal geometries fixed. Independent 3D RISM calculations were performed in an aqueous environment (cubic grids of 340^3 points with 0.3 Å spacing, second order partial series expansion closure, 298.15 K, TIP3P water model parameters, and conditions as in *(58)*) in order to yield the solvation free energies of the complex and the individual partners *(42, 58)*. Applying this procedure for 10 ALPB-optimized snapshots taken every 1 ns from the last available frames of RET^{wt}/AD80, RET^{wt}/AD57, and RET^{V804M}/AD80 simulations and adding the direct interaction energy of the complex partners yielded a "per snapshot" estimate of the binding free energy. These values were entered into a discrete canonical partition function expression by Boltzmann weighting, from which the final estimates of the ensemble binding free energy difference were computed. These can be compared to experimental values via $-RT \ln IC_{50}(\text{educt})/IC_{50}(\text{product})$, RT being the product of molar gas constant and temperature.

RNA sequencing

RNA was isolated from duplicates of LC-2/AD cells after 48 h treatment with 100 nM AD80 or DMSO controls using the RNeasy Kit (Qiagen) following the

manufacturer's protocols. RNA quality and integrity was verified using a Tapestation (Agilent Technologies). Strand-specific libraries were prepared using the TruSeq stranded mRNA sample preparation kit. Library preparation started with 1 µg total RNA. After poly-A selection (using poly-T oligo-attached magnetic beads), mRNA was purified and fragmented using buffer containing Mg^{2+} ions at 94 °C. The RNA fragments underwent reverse transcription using random primers. This was followed by second strand cDNA synthesis with DNA Polymerase I and RNase H. After end repair and A-tailing, indexing adapters were ligated. After purification, 10 µl template was used for amplification (14 PCR cycles) to create the final cDNA libraries. After library validation and quantification (Agilent 2100 Bioanalyzer), equimolar amounts of library were pooled. The pool was quantified by using the Peqlab KAPA Library Quantification Kit and the Applied Biosystems 7900HT Sequence Detection System. The pool was sequenced by using a HiSeq 3000/4000 PE Cluster Kit and a HiSeq 3000/4000 SBS Kit on an Illumina HiSeq 4000 sequencer with a paired-end (76x7x76 cycles) protocol. Reads were mapped to the hg19 reference genome with TopHat and to genomic features according to the Illumina iGenomes hg19 gene annotation with the GenomicsFeatures v1.22.13 package *(59, 60)*. Differential expression analysis was performed using DESeq2 v1.10.1 with standard parameters (except for independentFiltering=F) *(61)*. q-values were calculated from raw p-values by Benjamini-Hochberg FDR adjustment for multiple testing.

Gene set enrichment analysis

Genes were ranked based on the log fold change divided by the standard error of the log fold change to incorporate both direction and significance of treatment effects. To analyze effects on MAPK signaling, ranked lists were input into the GSEA Java

application pre-ranked tool and queried against gene sets including genes down-regulated (HALLMARK_KRAS_SIGNALING_DN) or genes up-regulated (HALLMARK_KRAS_SIGNALING_UP) by KRAS activation as defined by the Hallmark gene sets *(28, 62, 63)*. Genes contributing most to the enrichment score (core enrichment) were recorded and visualized.

Kinase selectivity score

To quantify the cytotoxic selectivity of compounds, we calculated a compound's cell line selectivity similar to the kinase selectivity score approaches proposed by Davis et al. and Karaman et al. *(64, 65)*. To this end, we defined the genotype of the most sensitive cell line per compound as the main target and termed the corresponding concentration the primary GI_{50}. In all cases, the altered gene of the most sensitive cell line was among the intended targets of respective inhibitors. Similar to the concept of a 'therapeutic window,' we then calculated for each compound the ratios of the other cell lines' GI_{50}s to the primary GI_{50} to estimate how much fold increase of concentration relative to the primary GI_{50} is possible before growth of cell lines with other genotypes is impaired. This analysis showed that the GI_{50} concentrations of compounds with known high selectivity such as BGJ398 and ceritinib could be increased by 94-fold and 230-fold, respectively, before viability of a second cell line was decreased by 50% **(fig. S3A,B)**. In contrast, for the known multi-kinase inhibitors vandetanib and cabozantinib, effects across other cell lines were already present at much lower ratios (**fig. S3A,B**).

Clustering of cell lines based on drug sensitivity

For visualization, cell lines were clustered based on GI_{50} values and depicted as a heatmap indicating compound sensitivities and genotypes.

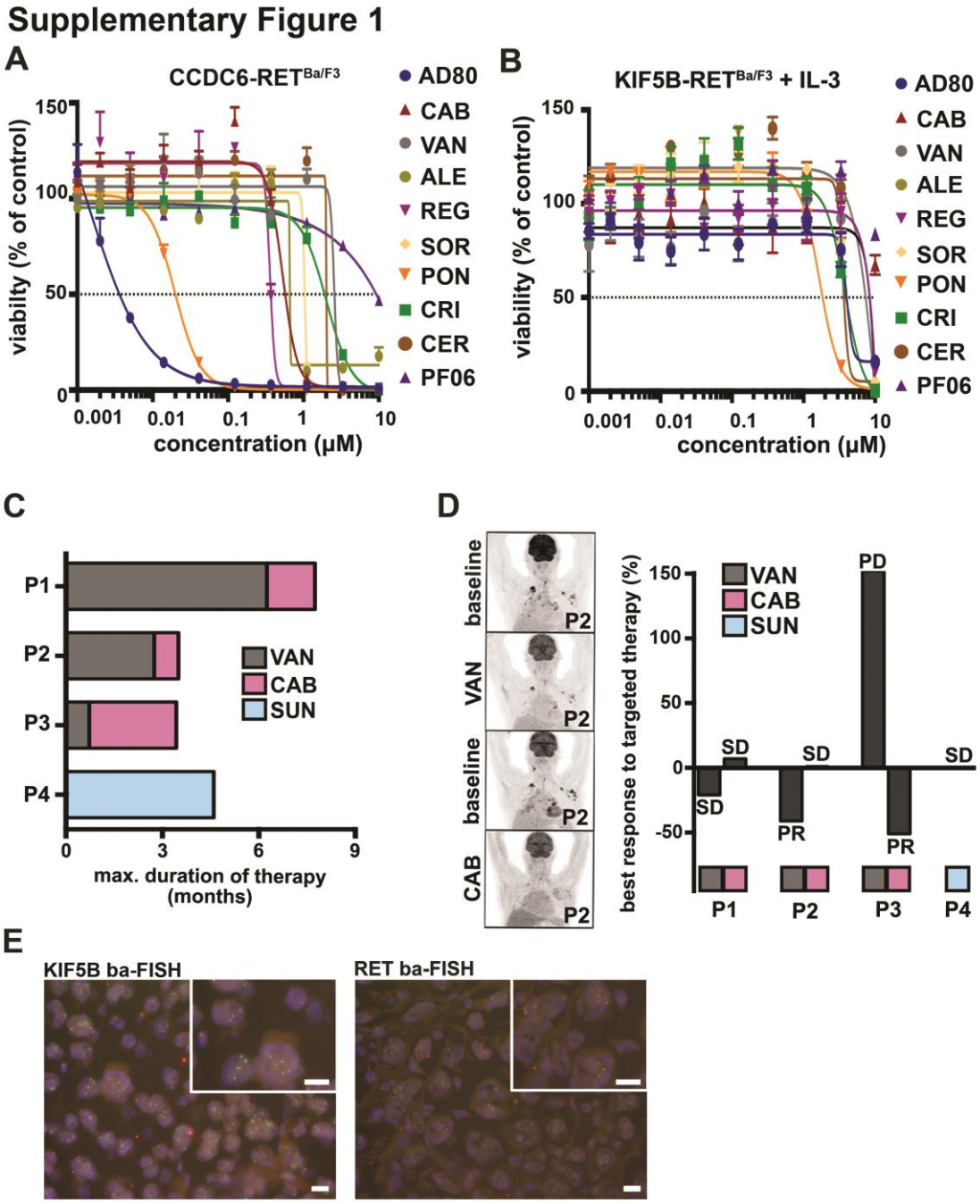

Fig. S1. Selective inhibition of signaling induced by rearranged RET and clinical activity in vivo.

A) Ba/F3 cells expressing *CCDC6-RET*^{wt} were treated (72 h) at increasing doses of AD80, PF06463922 (PF06), regorafenib (REG), crizotinib (CRI), sorafenib (SOR), ponatinib (PON), vandetanib (VAN), ceritinib (CER) or cabozantinib (CAB) and the corresponding viability curves were assessed. **B)** The same setting was used in Ba/F3 cells expressing *KIF5B-RET*^{wt} in the presence of IL-3 is shown. **C**) Time of treatment

for patients **(P1**-**P4)** on therapy with vandetanib (black), cabozantinib (rose), or sunitinib (light blue). **D**) Representative PET-CT scans of patient P2 **(P2)** showing best response of target lesions (left panel). Waterfall plots for best response of target lesions measured with PET/CT scans to vandetanib (black), cabozantinib (rose), or sunitinib (light blue) for each patient (right panel). PD: progressive disease; SD: stable disease; PR: partial response. **E)** Representative break-apart FISH (ba-FISH) images of *KIF5B* and *RET* probes for diagnostics of *RET* rearrangements in patient P3. Scale bars are equal to 10 μm.

Supplementary Figure 2

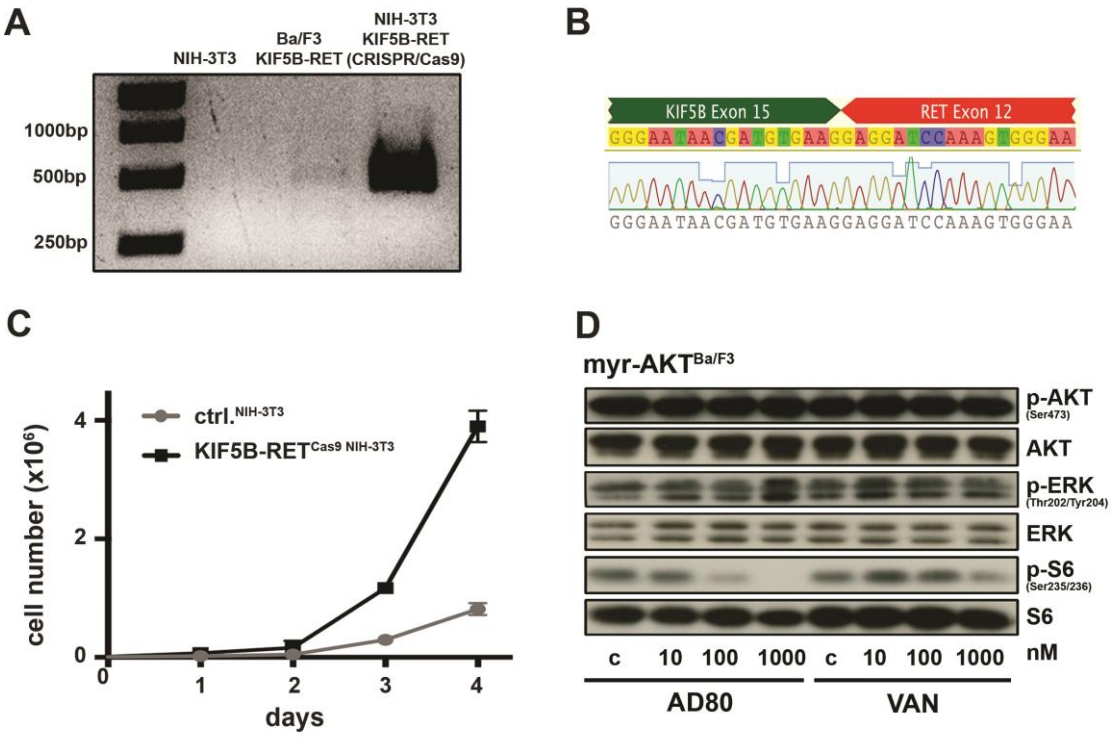

Fig. S2. Induction of *KIF5B-RET* rearrangements in NIH-3T3 cells via CRISPR/Cas9 and S6 kinase as an off-target of AD80.
A) The PCR product of the cDNA fusion transcript from NIH-3T3 cells with CRISPR/Cas9 induced *KIF5B-RET* fusion is displayed on an agarose gel. Parental NIH-3T3 cells and Ba/F3 cells expressing *KIF5B-RET* serve as control. **B)** Chromatogram from Sanger sequencing of NIH-3T3 cells with CRISPR/Cas9 induced *KIF5B-RET* rearrangement. **C)** Median cell number growth (up to 96 h) from consecutive measurements ± SD (n=3) comparing parental NIH-3T3 cells and NIH-3T3 cells with CRISPR/Cas9 induced *KIF5B-RET* fusion. **D)** Immunoblot of Ba/F3 cells expressing *myr-AKT* under AD80 or vandetanib (VAN) treatment (4 h).

Supplementary Figure 3

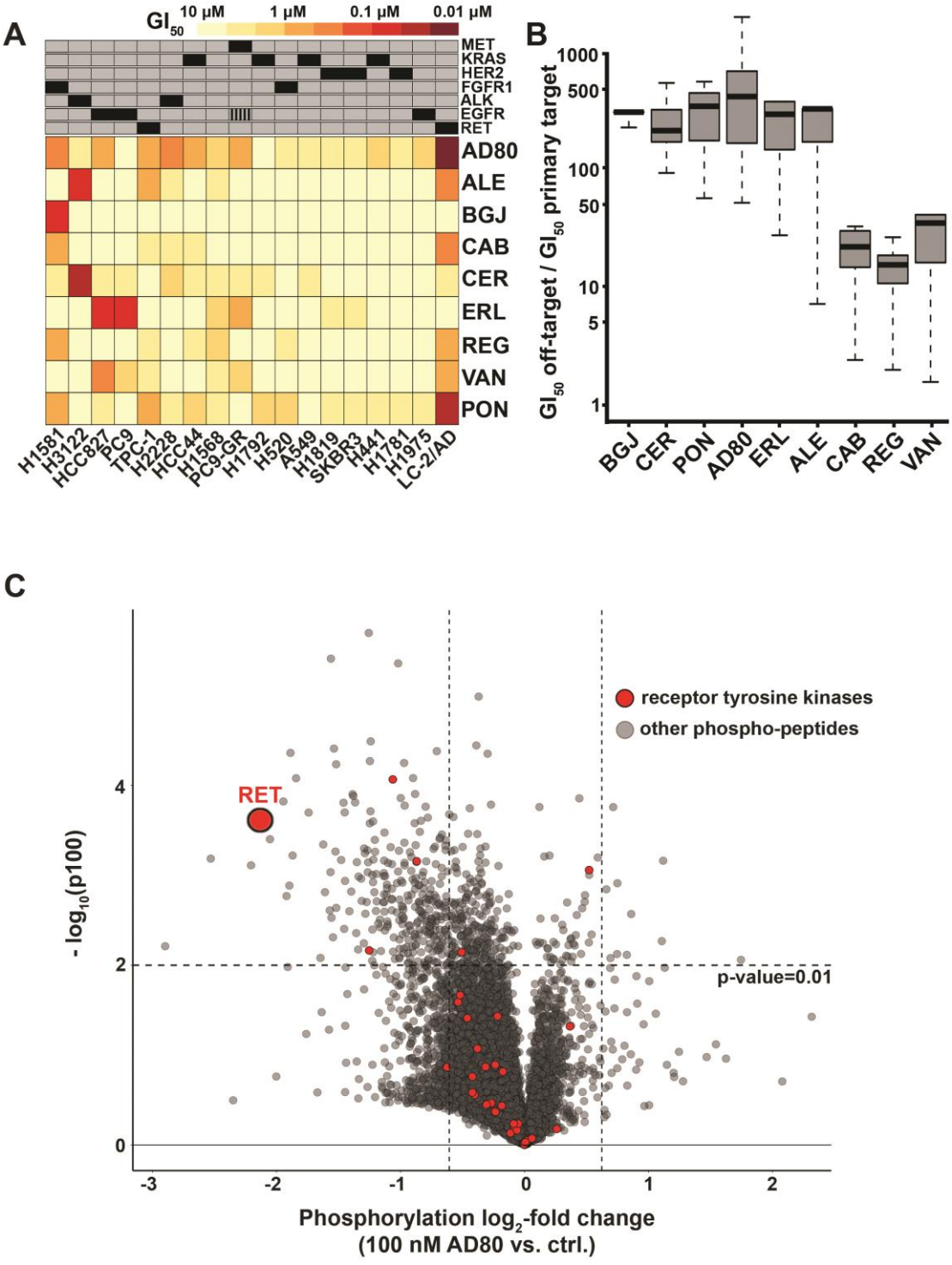

Fig. S3. Characterization of the activity profile of AD80.
A) Heat map of viability screening results from a panel of patient-derived cancer cell lines treated (72 h) with AD80, alectinib (ALE), BGJ398 (BGJ), cabozantinib (CAB), ceritinib (CER), erlotinib (ERL), regorafenib (REG), vandetanib (VAN), or ponatinib (PON). Results are shown as average GI_{50} values (n=3). The main oncogenic drivers are shown in the upper panel: *EGFR* mutant/ *MET* amplification (PC9-GR), *KRAS* mutant (H441; H1792; A549; HCC44), *HER2* overexpression (SKBR3; H1819), *Her2*

mutant (H1781), FGFR1 amplification (H1581; H520), *EML4-ALK* fusion (H3122; H2228), EGFR mutant (H1975; PC9; HCC827), *RET* fusion (LC-2/AD; TPC-1), and unknown (H1568). **B)** Box plot of ratios between GI_{50} values of cell lines with respective primary genotypic targets and non-target cell lines screened against the panel of inhibitors (n=3). **C)** Volcano plot depicting $\log_2$-change of phosphorylation change plotted against the $-\log_{10}$ p-values from phosphoproteomic analyses. Among all detected phospho-peptides, receptor tyrosine kinases are highlighted in red (n=3).

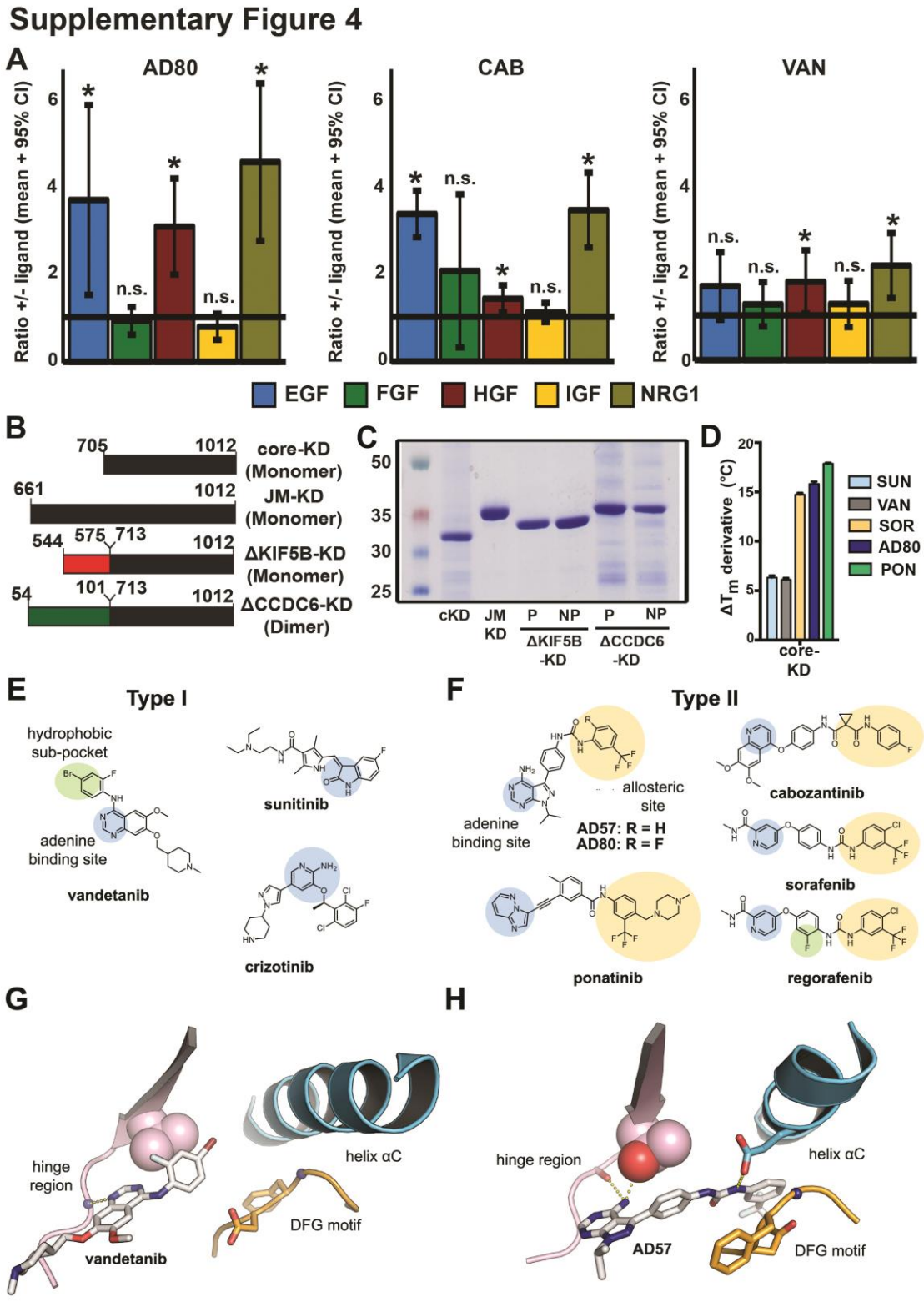

Fig. S4. Delineation of the cellular targets of AD80 using ligand screens and thermal shift experiments.

A) Effects of growth factor supplementation on the viability of LC-2/AD cells treated with indicated compounds. Bars indicate average across concentrations and experiments, error bars show 95% confidence intervals of the mean (n=4). **B)** Schematic presentation of the constructs used in the thermal stability assay: core kinase domain (cKD), juxtamembrane-kinase domain (JM-KD), truncated ΔKIF5B-

KD, and ΔCCDC6-KD, numbers correspond to amino acid position of RET wt. **C)** Coomassie stained SDS-PAGE gel of purified proteins: core kinase domain (cKD) 705-1012, juxtamembrane-kinase domain (JM-KD) 661-1012, truncated ΔKIF5B-KD, and ΔCCDC6-KD in a non-phosphorylated (NP) or phosphorylated (P) state. Molecular weight markers (kDa) are shown as indicated. **D)** Differences in melting temperatures from AD80, sorafenib (SOR), vandetanib (VAN), ponatinib (PON), or sunitinib (SUN) addition (ΔTm) and the respective standard errors of the mean (SEM) are shown for phosphorylated Core-KD. **E)** Overview of selected Type I kinase inhibitors and **F)** selected Type II kinase inhibitors with highlighted motifs addressing corresponding regions within the enzyme's binding site. **G)** Vandetanib (Type I) in complex with RET kinase (PDB-entry: 2IVU) and **H)** AD57 (Type II) in complex with cSRC (PDB-entry 3EL8).

Supplementary Figure 5

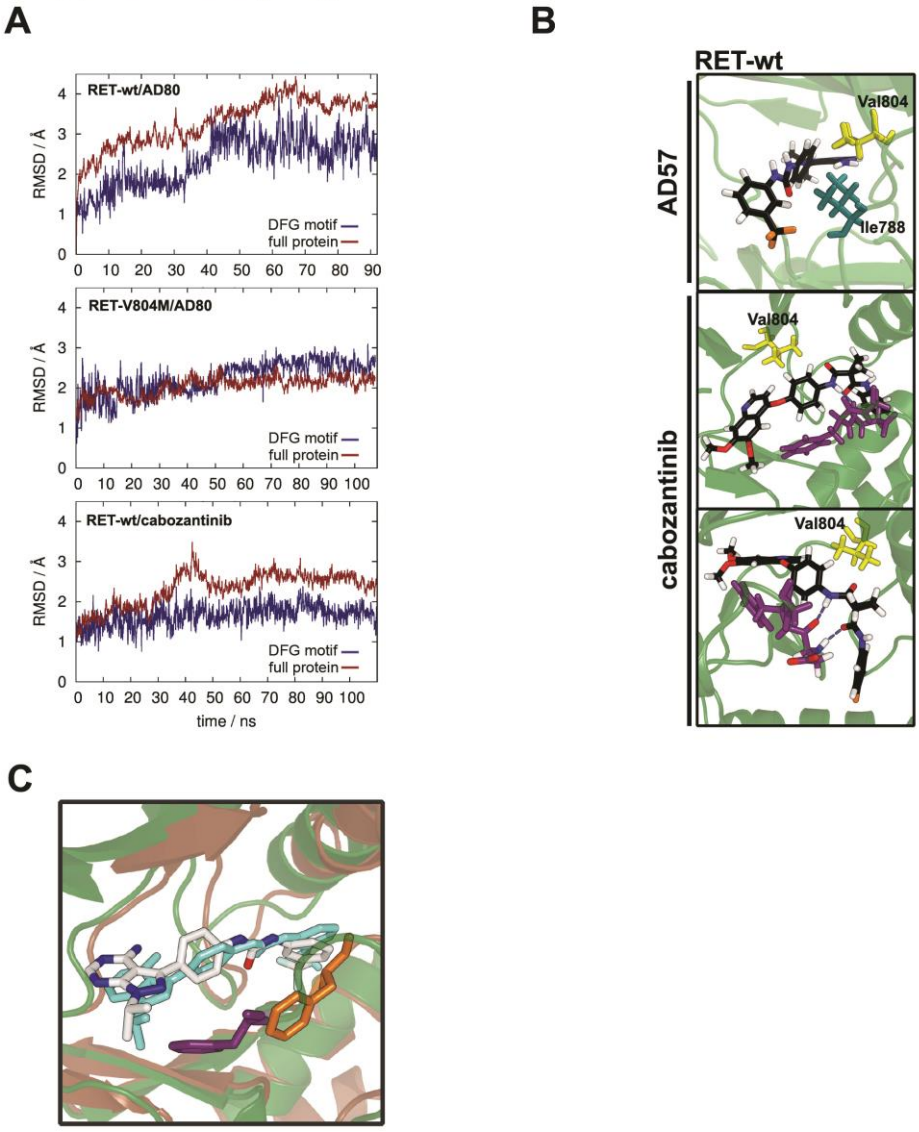

Fig. S5. RMSD of RET and AD80 or cabozantinib over time and ALPB-optimized structures.
A) RMSD of RET-wt (top, bottom) and RET-V804M (middle) with AD80 (top, middle) and cabozantinib (bottom) over simulation time, measured from the starting point of the respective simulations (middle and bottom data had been started approximately at the final top panel geometry). **B)** RET-wt/AD57 after 202 ns (92 ns from RET-wt/AD80 simulation followed by 110 ns TI-MD for gradually transforming AD80 into AD57, side view; top panel), RET-wt/cabozantinib after 112 ns from different perspectives, the latter allowing for H-bond identification (middle and lower panels). **C)** Superimposition of cSRC (brown, PDB code 3EL8) and RET-wt (green) in complex with AD57 (see also Fig. 3AII). The experimentally resolved ligand pose is shown in light blue with phenylalanine of the DFG motif in orange. The corresponding MD results are shown in element-specific colors for AD57 and in violet for Phe of DFG. Images have been created with PyMOL (The PyMOL Molecular Graphics System, Version 1.8 Schrödinger, LLC).

Supplementary Figure 6

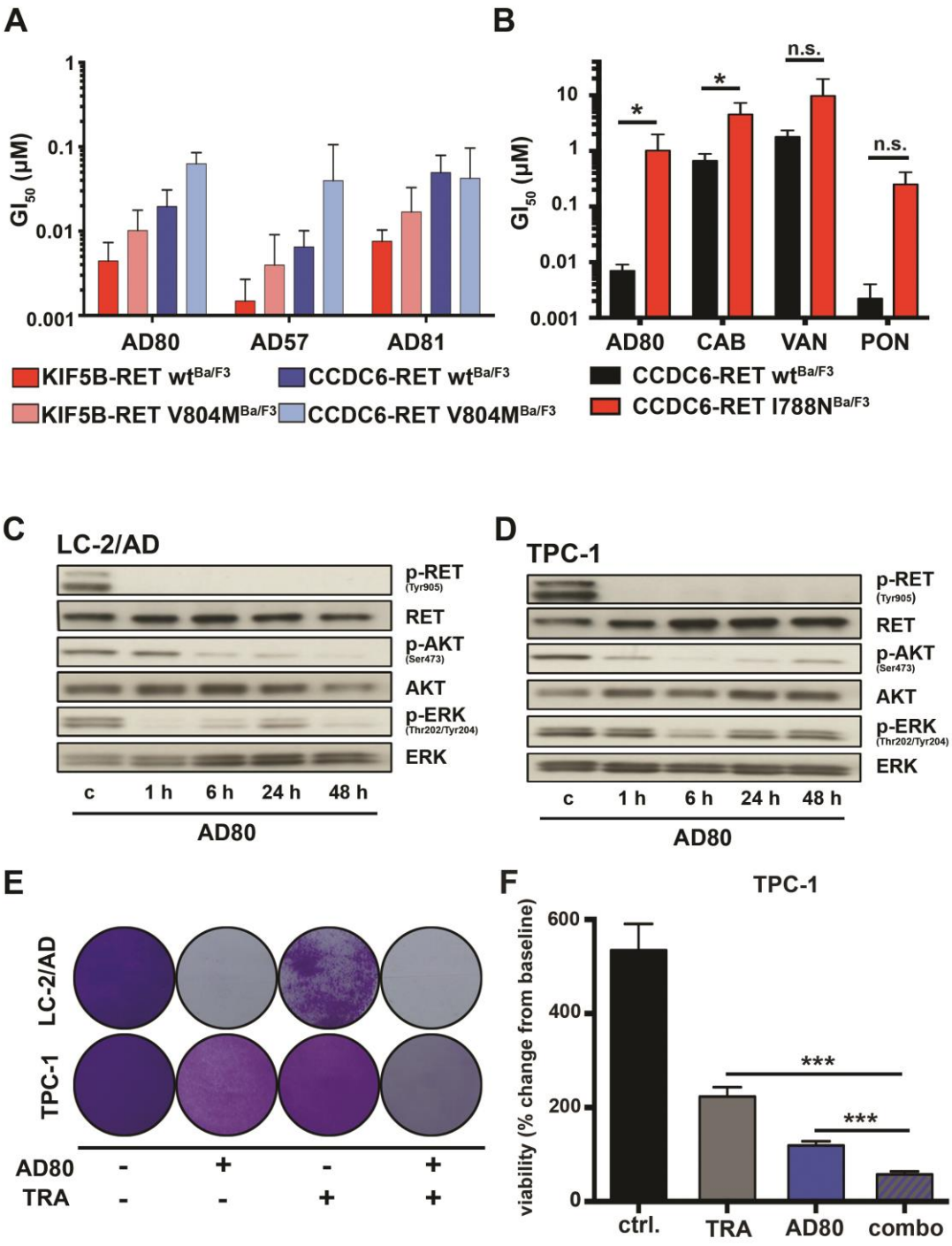

Fig. S6. Inhibitory potential of AD80 derivatives and resistance mechanisms against RET inhibition.

A) Column chart of mean GI_{50}-values + SD (n≥3) of Ba/F3 cells expressing wild type and V804M mutated *KIF5B-RET* or *CCDC6-RET* after 72 h of treatment with AD80 and AD80 derivatives AD57 and AD81. **B)** Column chart of mean GI_{50}-values + SD (n≥3) of Ba/F3 cells expressing CCDC6-RET^{wt} or CCDC6-RET^{V804M} after 72 h of treatment as assessed for AD80, cabozantinib (CAB), vandetanib (VAN), and

ponatinib (PON) is shown. **C)** Immunoblot of LC-2/AD cells treated with AD80 (0.1 µM) for 1 h, 6 h, 24 h, and 48 h. **D)** The same experimental setting was also applied to TPC-1 cells. **E)** Clonogenic assay of TPC-1 and LC-2/AD cells treated (7 d) with AD80 (0.5 µM), trametinib (0.5 µM), or a combination of both inhibitors. Cells are visualized via crystal violet staining. **F)** TPC-1 cells were treated (72 h) with AD80 (0.5 µM), trametinib (TRA) (0.5 µM), or a combination of both. Cellular viability was assessed and is given as mean % change from baseline (n=3).

Supplementary Figure 7

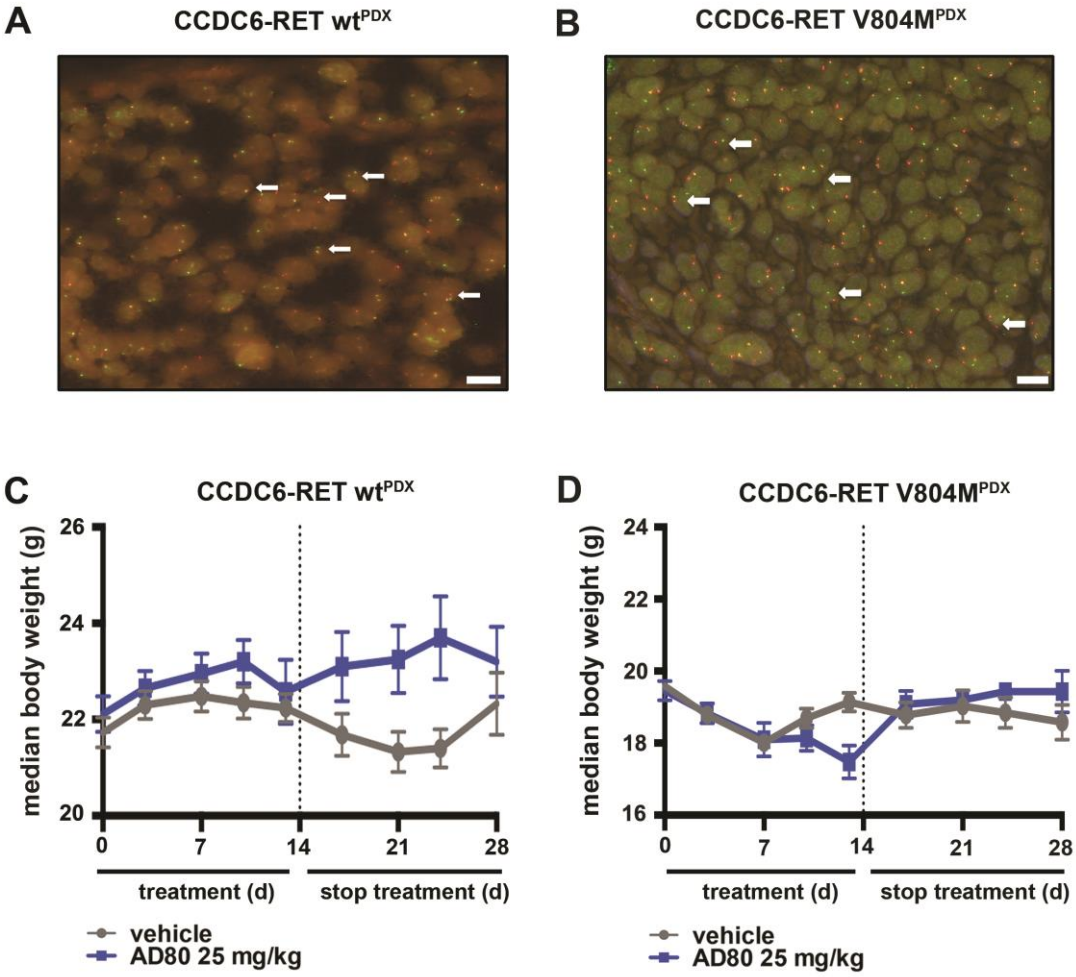

Fig. S7. Validation of PDX via fluorescent in situ hybridization (FISH) and in vivo effects induced by treatment with AD80.
A) A representative positive fluorescence in situ (FISH) break-apart analysis from mice engrafted with *CCDC6-RET* fusion positive patient-derived tumor tissue (CCDC6-RET^{PDX}) with split red and green signals, indicating RET gene rearrangements (white arrows). Scale bars are equal to 10 µm. **B)** A corresponding FISH analysis from CCDC6-RET V804M^{PDX}. **C)** Median body weight of CCDC6-RET^{PDX} treated with AD80 (25 mg/kg) or vehicle control and 14 days of follow-up. **D)** Median body weight for CCDC6-RET V804M^{PDX} under AD80 (25 mg/kg) and vehicle treatment.

Table S1. IC_{50} values of AD80, cabozantinib, and vandetanib for phospho-RET in Ba/F3 cells expressing wild type or V804M *KIF5B-RET*.
Overview of IC_{50} values of phospho-RET signal from displayed immunoblots of Ba/F3 cells expressing wild type or V804M *KIF5B-RET* treated with AD80, cabozantinib, and vandetanib.

Fitted IC_{50} values (nM) quantified from immunoblot

	AD80	**cabozantinib**	**vandetanib**
KIF5B-RET-wt	9.24	10.12	NA
KIF5B-RET-V804M	9.98	NA	NA

Table S2. Rates of clinical response to currently available anti-RET drugs and clinical information of patients used in retrospective analysis.
A) Publically available clinical data for progression-free survival (PFS) and objective response rates (ORR) from patients with *RET*-rearranged tumors treated with cabozantinib (NCT01639508; *(66)*) or vandetanib *(9)* and *(10)*. **B)** Best response rates to targeted therapy for each patient receiving vandetanib, cabozantinib, or sunitinib therapy relative to baseline. Response was annotated as "partial response" (PR), "stable disease" (SD), or "progressive disease" (PD) according to RECIST 1.1 criteria. The dosing of the individual drugs per patient is displayed. **C)** Overview of patients for *RET* rearrangement and detection method.

A

	Median ORR (%)	**Median PFS (months)**	**cohort size**
Drilon *et al.*	28	7	20
Gautschi *et al.*	37% (cabozantinib), 18% (vandetanib), 22% (sunitinib)	2.3	53
Yoh *et al.*	53	4.7	17

B

	vandetanib	**cabozantinib**	**sunitinib**
dosage	300 mg/d	140 mg/d	**50/mg/d** (4 weeks on -2 weeks off); since cycler III dose reduction to **37.5 mg/d**
P1	-21% (PR)	7% (SD)	-
P2	-41 (PR)	1% (SD)	-
P3	152% (PD)	-51% (PR)	-
P4	-	-	0% (SD)

C

Patient	**ba-FISH RET**	**ba-FISH KIF5B**	**hybrid capture-based next generation sequencing**
P1	positive	positive	confirmation of KIF5B-RET rearrangement
P2	positive	negative	
P3	positive	positive	
P4	positive	positive	

Table S3. GI_{50} values of the panel of patient-derived cell lines.

A tabular overview of mean GI_{50} values (from n=3) from various patient-derived cancer cell lines treated (72 h) with AD80, alectinib (ALE), BGJ398 (BGJ), cabozantinib (CAB), ceritinib (CER), erlotinib (ERL), ponatinib (PON), regorafenib (REG), or vandetanib (VAN). GI_{50} values are given in μM.

Mean GI50 (μM) values from n=3

Cell Line	AD80	Alectinib	BGJ398	Cabozantinib	Ceritinib	Erlotinib	Ponatinib	Regorafenib	Vandetanib
SKBR3	2.800	>10	>10	>10	>10	3.300	3.881	4.900	9.600
H1781	1.800	>10	>10	>10	7.200	5.300	3.559	9.834	9.900
H1819	3.200	>10	>10	>10	5.600	2.000	4.151	5.834	8.500
H2228	0.280	3.300	7.400	3.906	1.700	9.700	3.797	6.400	>10
H520	2.800	>10	>10	8.888	8.500	>10	0.835	3.967	4.500
H1975	1.700	>10	>10	>10	5.900	6.100	3.357	5.891	>10
PC9-GR	0.710	7.400	>10	7.268	2.900	0.720	5.702	6.884	1.600
H441	1.400	>10	>10	9.156	4.600	5.300	3.458	7.749	4.300
A549	3.267	>10	>10	5.366	3.436	>10	4.968	5.622	>10
H1568	0.900	2.800	>10	4.740	3.400	1.500	2.294	1.141	2.100
LC-2/AD	0.004	0.215	>10	0.303	1.811	4.468	0.010	0.723	0.372
TPC-1	0.340	0.664	>10	1.992	5.990	9.502	0.333	2.375	3.901
H3122	1.777	0.030	>10	6.725	0.018	>10	5.287	5.136	>10
H1581	0.210	5.225	0.032	0.721	1.766	>10	0.574	0.369	5.275
H1792	8.134	>10	>10	6.689	4.075	>10	1.008	5.713	>10
HCC827	0.679	7.858	>10	4.474	3.877	0.026	2.118	7.011	0.241
PC9	6.582	>10	>10	5.946	3.133	0.038	5.151	8.907	1.366
HCC44	0.415	>10	>10	3.674	3.913	>10	1.455	3.215	>10

Table S4. Tabulated derivative melting temperatures (T_m) and differences in melting temperature (ΔT_m) values.

Derivative melting temperatures (Tm) and differences in melting temperatures (ΔTm) and the respective SEM variance are shown. Proteins were incubated with 1 μM drug or equivalent volume of DMSO before the experiment. Non-phosphorylated forms of each RET protein were extensively CIP-phosphatase treated to remove phospho-tyrosine. To activate the proteins, they were incubated either with Mg-ATP or with Mg-ATP and an active RET kinase protein to drive autophosphorylation. Thermal shift experiments were performed using two to five independent preparations of each protein and were carried out in triplicates.

Protein	Drug	Tm derivative		ΔTm derivative	
		Non-phosphorylated	Phosphorylated	Non-phosphorylated	Phosphorylated
ΔCCDC6-RET	no drug	48.09 ± 0.19	47.81 ± 0.08	0.00 ± 0.00	0.00 ± 0.08
	sunitinib	52.73 ± 0.96	52.33 ± 0.14	4.64 ± 0.77	4.52 ± 0.14
	vandetanib	52.86 ± 0.65	52.61 ± 0.05	4.76 ± 0.45	4.80 ± 0.05
	sorafenib	58.19 ± 0.76	58.50 ± 0.17	10.10 ± 0.56	10.69 ±0.17
	AD80	59.02 ± 1.48	62.73 ± 0.06	10.93 ± 1.29	14.92 ± 0.06
ΔKIF5B-RET	no drug	45.40 ± 1.24	45.08 ± 0.72	0.00 ± 0.00	0.00 ± 0.00
	sunitinib	46.99 ± 2.27	47.52 ± 1.81	1.59 ± 1.02	2.44 ± 1.45
	vandetanib	49.28 ± 1.77	49.67 ± 2.03	3.88 ± 0.53	4.59 ± 1.64
	sorafenib	58.31 ± 0.11	58.69 ± 0.16	12.91 ± 1.35	13.61 ± 1.05
	AD80	61.79 ± 0.56	62.58 ± 0.24	16.39 ± 0.68	17.50 ± 0.68
JM-KD	no drug	41.78 ± 1.38	41.89 ± 0.54	0.00 ± 0.00	0.00 ± 0.00
	sunitinib	44.08 ± 2.07	42.55 ± 0.38	0.93 ± 0.01	0.70 ± 0.80
	vandetanib	44.22 ± 1.96	44.93 ± 0.50	1.48 ± 0.40	3.08 ± 0.68
	sorafenib	54.44 ± 1.43	56.33 ± 0.61	12.66 ± 0.07	14.66 ± 0.23
	AD80	54.36 ± 1.56	56.83 ± 0.76	12.58 ± 0.26	14.94 ± 0.71
Core KD	no drug	42.78 ± 0.27	43.01 ± 0.06	0.00 ± 0.27	0.00 ± 0.06
	sunitinib	46.25 ± 0.19	49.34 ± 0.21	3.47 ± 0.19	6.33 ± 0.21
	vandetanib	45.39 ± 0.11	49.11 ± 0.19	2.61 ± 0.11	6.11 ± 0.19
	sorafenib	56.18 ± 0.15	57.74 ± 0.18	13.39 ± 0.15	14.73 ± 0.18
	AD80	55.35 ± 0.20	58.82 ± 0.24	12.57 ± 0.20	15.81 ± 0.24

Core KD	-	ATP	AD80	cabozantinib	ponatinib	sorafenib
Ave TM	42.28	46.96	55.22	57.01	61.24	55.85
st dev	0.29	0.00	0.72	0.29	0.18	0.18
st err	0.15	0.00	0.41	0.15	0.09	0.09
Ave dTM	0.00	4.67	12.69	13.92	17.87	13.20
st dev	0.29	0.00	0.75	0.34	0.18	0.18
st err	0.15	0.00	0.43	0.17	0.09	0.09

Table S5. In vitro kinase assay of RET^{wt}, RET^{V804M}, and RET^{V804L} mutants with different inhibitors.

An overview of IC_{50} values of a panel of type I and II RET inhibitors determined by homogeneous time-resolved fluorescence (HTRF) in vitro kinase assay.

type of binding	compound	RET wt IC 50 [nM]	RET V804M IC 50 [nM]	RET V804L IC 50 [nM]
type II	AD80	1.3 ± 0.2	0.4 ± 0.2	0.6 ± 0.3
type II	ponatinib	3.4 ± 0.2	4.7 ± 0.1	4.2 ± 0.3
type I	crizotinib	12.5 ± 0.9	90.9 ± 17.2	108.4 ±18.4
type II	cabozantinib	23.7 ± 7.9	209.5 ± 8.6	150.0 ± 22.9
type I	sunitinib	30.5 ± 11.9	74.9 ± 19.7	69.0 ± 13.1
type II	sorafenib	63.7 ± 26.8	21.5 ± 6.5	32 ± 3
type I	vandetanib	382.3 ± 23.9	>2000	>2000

Table S6. Experimental setup for saturated mutagenesis screening.
An overview of the experimental setting for our saturated mutagenesis screening using XL1-RED *E. coli* is given. The primary RET construct transformed in XL1-RED E. coli, the duration of accelerated mutagenesis in these cells, the AD80 concentration at which transduced Ba/F3 cells were selected, and the deep sequencing results are shown.

Primary RET construct	duration of mutagenesis (h)	AD80 selection (nM)	cDNA change	protein change
CCDC6-RET	24	200	-	-
KIF5B-RET	48	200	-	-
CCDC6-RET	72	200	2363 T>A	I788N